Journal of Engineering and Sustainable Development
Vol. 30, No. 01, January 2026
https://jeasd.uomustansiriyah.edu.iq/index.php/jeasd
ISSN 2520-0917
Research Article
https://doi.org/10.31272/jeasd.2589

Numerical Study of Predicting Solar Air Collector Dimensions to Achieve the Optimum Performance

Ahmed Hammodi Abd[1*], Hazim A. Al-Zurfi[1], Layth Mustafa Salman[1], K. Sopian[2]

[1]Department of Technical Power Mechanics, Al-Najaf Technical Institute, Al-Furat Al-AwsatTechnical University (ATU), Najaf, Iraq
[2]Solar Energy Research Institute (SERI), University Kebangsaan Malaysia, 43600 Bangi, Selangor, Malaysia

*Email: Ahmed.adod.inj@atu.edu.iq

Article Info

Received	17/04/2024
Revised	24/11/2025
Accepted	13/12/2025

Abstract

The primary objective of this work is to develop and evaluate a computational model to predict the fluid-flow and heat-transfer properties of a reverse-flow corrugated solar air heater collector, with or without a thermal storage unit. ANSYS 19.0 is used for many applications. This study also included an analysis of digital systems and their application to solving the continuity, momentum, and energy equations. These equations were solved numerically using the finite volume method. In this work, the thermal performance of a flat-plate solar collector with fixed dimensions (length = 1.8 m, width = 0.7 m, channel height = 0.07 m) was evaluated, using air as the working fluid. Temperature differences were measured and plotted against air mass flow rates. The results showed temperature differences across air mass flow rates (0.03-0.06 kg/s) at a solar irradiance of 1000 W/m². For each increase in air mass flow rate, a corresponding decrease in the air temperature difference was observed, ranging from 26.9 °C to 14 °C for mass flow rates of 0.03 and 0.06 kg/s, respectively. This was based on numerical analysis of the solar collector; it has been shown that the thermal efficiency increases with the air mass flow rate.

Keywords: Nanoparticles, Numerical, Optimum dimensions, Paraffin wax, Solar air collector

1. Introduction

Recently, a significant increase in the global population, particularly in Iraq, has been observed. This has led to a surge in electricity demand, resulting in increased fossil fuel consumption and, consequently, higher greenhouse gas emissions. These emissions contribute significantly to global warming and water scarcity, problems that affect the world in general and Iraq in particular. This has prompted scientists to explore viable alternatives, including renewable energy sources such as solar and wind power, as a secondary energy source [1]. Relying on renewable energy has become essential today, given its significant role in supporting and boosting national economies. Among the most prominent forms of this energy is solar power generation, with concentrated solar power technology, particularly solar tower technology, being a beautiful solution due to its ease of operation, simple maintenance requirements, and long lifespan, which can extend up to one hundred years. Because of the abundant sunlight reaching Earth each day, solar energy is a leading renewable energy source [2].

Improving the performance of solar systems without a storage unit has been studied in numerous studies, employing several methods to enhance flow turbulence or increase the heat-transfer rate. In this work, a computational model was developed to predict the fluid-flow and heat-transfer characteristics of a corrugated-flow solar air heater collector. Reverse, with or without including a thermal storage unit. The systems were numerically simulated using ANSYS 19.0. It was also used to solve the governing continuity, momentum, and energy equations using the conventional finite-volume numerical method. The thermal performance of a flat plate made of the material SAH, with fixed dimensions of length and width (L = 0.7, W = 1.8) meters, was investigated. The channel height (Hch = 0.07 m) was evaluated. Using an air-base fluid, air temperature differences were collected and plotted against air mass flow rates.

Lin et al. [3] developed a numerical model of a cross-corrugated solar air heater collector. The model consists of wavy plates from the absorber and the bottom sides. It was found that the thermal performance of the proposed model is significantly higher than that of the flat-plate collector, and the use of wavy

plates led to an improvement in the thermal efficiency of the solar air heater. El-Sebaii et al. [4] published an experimental work to evaluate the performance of a solar air collector employing four distinct absorber surface shapes: a flat plate surface, a corrugated surface, a protrusion surface, and a corrugated surface with a protrusion. Therefore, the author indicated that the highest heat transfer was achieved when the corrugated plate was used as the absorber surface. To compare and contrast the efficiency of two types of solar air collectors—one with a finned design and the other with a corrugated one—conducted both theoretical and experimental work.

It has been noted that the maximum thermal efficiency of a corrugated solar air collector is 17.4% higher than that of a finned solar air collector. Moreover, the outlet temperature of a corrugated solar air collector is increased by 2.1 % - 9.7 % more than that of a finned solar air collector. Numerical simulation has been carried out by Karim et al. [5] to work on the influence of a set of parameters on the performance evaluation of corrugated solar air collectors with a single and double airflow channel. The results of this numerical simulation indicate that solar irradiance, wind speed, air mass flow rate, and input air temperature have the same influence on the performance of both single-and double-airflow channels. Additionally, the impact of collector length varies substantially between single- and double-airflow channels due to differences in airflow within the channels.

An experimental study of an unglazed solar air collector with a perforated flat-plate absorber for heating a building under the climatic conditions of western Iraq was conducted by A. Al-Damook and Khalil [6]. The authors found that the maximum temperature difference is 6 °C on cloudy days and 17 °C on sunny days at solar noon [7]. Hassan and Abo-Elfadl [8] for the performance evaluation of a solar evacuated tube collector for space heating buildings. The studies were conducted under the climatic conditions in Baghdad, Iraq, over five months, from early November to the end of March. The results of this work indicate that the maximum thermal efficiency of 37.75% was achieved in December. This study analyzes the thermal performance of building-integrated photovoltaic systems, with particular attention to heat-transfer mechanisms within the building envelope. The research methodology combines computer simulations and experimental testing to evaluate the efficiency of these systems and their role in improving building energy efficiency.

Charvat et al. [9] conducted experimental investigations to assess the impact of jet impediment on the performance of a corrugated solar air heater and to compare it with that of a flat solar air heater. The author has demonstrated that the corrugated plate yields an average thermal efficiency of 14% with a 3 °C temperature increase, which is higher than that of the flat plate of the solar air heater. Experimental performance analysis of the solar air collector was also conducted by Zauner et al. [10] using four various absorber surface shapes: flat plate, pin finned, corrugated perforated finned, and corrugated finned. Hence, the results reveal that the maximum thermal efficiency of the solar air collector was achieved with the corrugated, perforated, finned surface.

The primary issue with solar energy is its intermittency, even though the energy it provides is more reliable than that of other renewable sources. Thermal energy storage is considered an optimal remedy for the intermittency of solar energy, as it is dependent on the duration of solar irradiation. Thermal energy storage is practical because it increases efficiency in both energy conservation and solar heating [11]. Consequently, numerous studies suggest that various types of PCMs may benefit from solar systems that incorporate thermal energy storage units.

Vijayan et al. [12] simulated two distinct kinds of solar air collectors using numerical methods: front-flow and back-flow. An example of the former is a solar collector that uses a thin metal plate (0.5 mm) with a thermal conductivity of 40 W/m.K. and is designed to be lightweight; an example of the latter is a PCM-based solar collector. PCM's latent heat is 180 kJ/kg, and its melting point is 40 °C. By simulating heat transport in PCM using MATLAB and TRNSYS, the authors conduct a thorough evaluation of the air collector model's performance. During the day, the air temperature at the solar collector outlet will decrease due to thermal energy storage in the PCM, as shown by numerical calculations. Additionally, the findings demonstrated that the release of heat stored in the PCM at night increases the ambient temperature. A solar air collector that incorporates a PCM-filled packed bed of spherical capsules was the subject of an experimental investigation by Ali et al. [13]. Nighttime measurements by the author reveal that the solar air collector maintains a consistent heat-discharge process. The author also reported a daily energy-efficiency range of 32%-45% for the solar air collector. Experimental and numerical analyses were performed by Lakshmi et al. [14] to develop a solar energy system using a hybrid latent-sensible thermal stPCM storage material.

The solar system primarily consists of a shell-and-tube heat exchanger. The phase change material is filled in the tubes, and thermal oil is used as the heat-transfer medium. They found that the power of the sensible thermal oil section of the storage is slightly affected, whereas the power of the phase change material section increases significantly. Although the thermal response of oil was faster than that of phase change material, on the other hand, the thermal conductivity of the phase change material was steadier. Accordingly, the time required to discharge the stored thermal energy is reduced. They also found good agreement between the experimental and numerical results. Thus, the model could be developed through numerical analysis.

Alva et al. [15] conducted an experimental investigation into the performance of a sensible thermal energy storage system using a flat-plate solar air collector. Its storage media consisted of gravel and iron scraps. The findings demonstrate that, compared with a solar air collector without a thermal storage unit, one with a thermal storage unit had a thermal efficiency that was 10%-15% higher. Experimental and mathematical analyses were performed by Vijayan et al. [12] on a solar air collector integrated with gravel for dehydrating bitter gourd. It was found that seven hours were required to reduce the gourd's humidity from 92% to 9%, whereas ten hours were needed to dry it under direct sunlight. The average efficiencies of the solar

collector and dryer were 22% and 19%, respectively [16]. Mahmud et al. [17] conducted an experimental study on a dual solar air collector, with and without thermal energy storage systems, and a matching storage system.

Alkilani et al. [18] conducted an experiment investigating the performance of a corrugated solar air collector integrated with gravel as a sensible storage medium beneath the corrugated absorber plate. The results reveal that the maximum energy and exergy efficiencies for the solar air collector were 58.16% and 14.6%, respectively. Dhaidan et al. [19] presented a performance analysis of a thermal energy storage system, focusing on the charging and discharging periods. It was found that the energy efficiency value depends on initial temperature and flow rates. They also found energy efficiencies of 54.48%, 56.05%, and 68.26% at flow rates of 0.010 kg/s, 0.012 kg/s, and 0.014 kg/s, respectively.

Enhancing thermo-physical properties is one of the most effective methods for improving thermal energy storage systems [20]. Materials that store heat have a high thermal conductivity, which is a crucial quality. Hence, thermal energy storage materials are modified by incorporating nanoparticles to enhance their thermo-physical properties [21]. This study focuses on the use of rectangular, double-edged, corrugated metal strips to enhance the thermal performance of flat plate solar collectors. The results indicate that this design improves heat-transfer efficiency relative to conventional designs. High operating temperatures often reduce the efficiency of solar cell systems. To address this issue, several cooling strategies have been explored; in particular, backside cooling systems using phase change materials (PCMs) and heat dissipation devices have shown promising results in improving the thermal performance of these systems [22].

Table 1 summarizes investigations into the mixing of nanoparticles with thermal energy storage materials used in solar energy systems. Specifically, it summarized the information in terms of the type of storage medium, the type of nanoparticles, size, mass or volume fractions, and highlighted the results. In the literature, the corrugated absorber plate surface is considered the most efficient due to its increased cross-sectional area, thereby enhancing heat transfer between the absorber surface and the working fluid. The present work concludes that sensible heat storage is inferior to latent heat storage using PCM because the latter has lower temperature gradients during melting and freezing, and the former has a higher thermal energy storage density. Among polycrystalline minerals (PCMs), paraffin excels in thermal energy storage due to its superior characteristics. That said, paraffin's low thermal conductivity reduces storage efficiency. Hence, compared with pure paraffin wax, adding nanoparticles to paraffin wax improves thermal conductivity and storage efficiency by reducing the thermal barrier to heat transfer between the surface and the paraffin wax.

Table 1. Physical properties of paraffin wax [4]

Property	Quantity
Penetration at25ºc	34
Oil content wt%(max)	1.5
Melting point aroundº c	38
Color (SAYBOLT)(min)	20

2. Method Of the Research

2.1 Physical Model and Assumptions.

The physical model of the single-pass solar air heater with and without a thermal energy storage system is described in detail after implementing the following assumptions in the numerical analysis:

- The system operates in steady state conditions.
- The air flowing is incompressible.
- The heat flux is uniform.
- The air flow channel is free of leakage.
- The system is designed as a three-dimensional.
- The PCM is considered in direct contact with the absorber plate surface.
- The PCM volume variation is ignored during phase change.
- The thermo-physical properties of air, PCM, and Nano-PCM are considered constant during operation of the system.
- The liquid phase of the PCM and Nano-PCM is considered incompressible and Newtonian.

The system configuration of the solar air collector without storage is shown in Fig. 1. The solar air collector uses a corrugated plate surface made of mild aluminum, painted black to increase solar irradiance absorption and reduce thermal reflectivity. A transparent glass plate covers the top surface to reduce convective heat losses. The collector is insulated with glass wool on the bottom and lateral sides to reduce thermal losses. The body is made of 16mm plywood. The airflow channel has dimensions of 1.8m, 0.7m, and 0.07m in length, width, and height, respectively. The collector has an average gap spacing of 4.83 cm. The absorber plate is designed with seventeen equilateral-triangle containers in which the PCM is placed, as in Fig. 2.

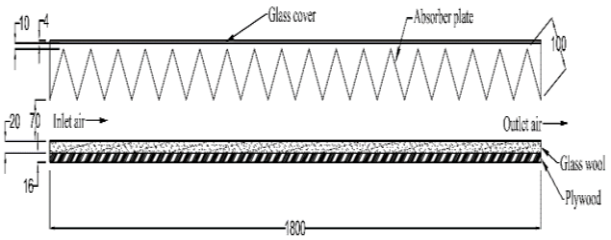

Figure 1. Schematic view of the system configuration of a solar air collector without storage.

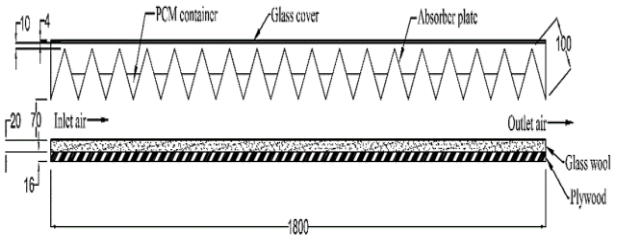

Figure 2.A schematic diagram illustrating the integrated structure of a solar air collector system equipped with a thermal storage unit, showing the main components and the heat and air flow paths within the system.

2.2 CFD Modeling Process.

In essence, one could approach a CFD problem by adhering to the general procedure stages of the modeling process. The commercial software utilized in the present work to compute the efficacy of the solar air heater collector is ANSYS R19.0. As in Fig. 3.

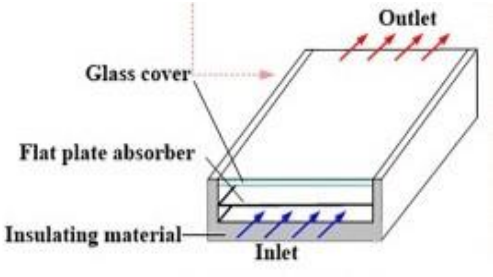

Figure 3. General model heat transfer [23]

2.3 Governing Equations

ANSYS Fluent is a commercial software package used to perform numerical simulations of forced-convection heat transfer in the SAH. The numerical simulations have been performed by using a steady-state pressure-based solver. The governing partial differential equations for mass and momentum have been solved for steady incompressible flow, and the Semi-Implicit Method for Pressure-Linked Equations (SIMPLE) technique has been applied for numerical computations, with second-order upwind methods used to achieve pressure-velocity coupling in the governing equations. Finalising numerical SAH analysis requires the governing equations for motion, energy, and continuity. The energy equation, the stable (3-D) form of the continuity equation, and the time-averaged incompressible Navier-Stokes equations govern the phenomena under investigation. These equations may be expressed in terms of the Cartesian tensor system [23].

2.4 Continuity Equations

The continuity equation expresses the principle of conservation of mass in a flow; it requires that the sum of the masses entering and leaving any given volume per unit time equals the rate of change of mass resulting from changes in density over the same period. It can be formulated mathematically by equations (1, 2, and 3) below, respectively.

$$\rho \frac{\partial}{\partial x_i}(u_i) = 0 \qquad (1)$$

Momentum equation:

$$\frac{\rho \partial (u_i u_j)}{\partial x_i} = -\frac{\partial p}{\partial x_i} + \frac{\partial}{\partial x_j}\left[\mu\left(\frac{\partial u_i}{\partial x_j} + \frac{\partial u_j}{\partial x_i}\right)\right] + \rho \frac{\partial}{\partial x_j}(-\overline{u_i' u_j'})$$

(2)

Energy equation:

$$\rho \frac{\partial}{\partial x_i}(u_i T) = \frac{\partial}{\partial x_j}\left[(\Gamma + \Gamma_t)\frac{\partial T}{\partial x_j}\right] \qquad (3)$$

Whereturbulent theand the molecular thermal diffusivity Γ thermal diffusivity are given by the following equations (4 and 5):

$$\Gamma = \frac{\mu}{p_r} \qquad (4)$$

$$\Gamma_t = \frac{\mu_t}{p_{rt}} \qquad (5)$$

An appropriate turbulence model must be used to determine the turbulent viscosity term. The turbulent viscosity may be expressed as equation (6):

$$\mu_t = \rho C_\mu \frac{k^2}{\varepsilon} \qquad (6)$$

2.5 Boundary Conditions

The solution to the present problem, defined geometrically by a schematic representation and mathematically by governing equations, requires the specification of appropriate boundary conditions for the computational domain. Then, boundary conditions such as inlet air-velocity condition (air mass flow rate), heat-flux condition, absorber-plate condition, outlet air-flow condition, and PCM condition inside the containers are specified. The 3-D computational domain with continuity, momentum, and energy equations for numerical analysis. The flow behavior of each application can be better understood using turbulence models. Choose the renormalized group turbulence model and the conventional turbulence model [24],[25]. Apply the finite volume approach to the work of the turbulence model and the independent incompressible Navier-Stokes equations. Coupled Algorithm for Pressure and Velocity. Second-order upwind schemes were used for the solution, and the Semi-Indirect Method for Pressure-Linked Equations for Pressure Field Evaluation (SIMPLE) was employed.

3. Results and discussion.

The results of numerical analysis simulation by software (ANSYS 19.0) were presented to show both the temperature

distribution and the fluid flow of the three different configurations of SAH. The system's thermal performance is given, and comparisons across parameter conditions are provided to investigate the thermal efficiency of the SAH system. Accordingly, the results of all designs in the current numerical analysis are summarized in Table 2, which compares the designs with respect to Tin, Tout, T, and.

Table 2. Thermodynamic variation of an SAH with the following dimensions (L=1.8 m, W=0.7 m, Hch= 0.07 m) subjected to varying air mass flow rates and 1000 W/m2 sun irradiation

Design	$\dot{m}$ (kg/s)	T_{in} (°C)	T_{out} (°C)	ΔT (°C)	η_{th} (%)
Flat Plate SAH	0.03	25	51.9	26.9	64
	0.04	25	45.5	20.5	65
	0.05	25	41.6	16.6	66
	0.06	25	39.0	14.0	67
Corrugated SAH without Storage	0.03	25	87.0	62.0	74
	0.04	25	73.3	48.3	77
	0.05	25	64.2	39.2	78
	0.06	25	58.1	33.1	79
Corrugated SAH with PCM	0.03	25	69.0	44.0	69
	0.04	25	59.0	34.0	71
	0.05	25	52.8	27.8	73
	0.06	25	48.5	23.5	74
Corrugated SAH with Nano-PCM	0.03	25	71.4	46.4	73
	0.04	25	61.6	36.6	76
	0.05	25	54.5	29.5	77
	0.06	25	50.0	25.0	78
	0.06	25			

3.1 Optimal Collector Dimension Prediction for Temperature Rise.

The objective of this work is to determine the optimal dimensions of a solar air heater (SAH) collector, including the length, width, and depth of the air-flow channel, to maximize the increase in the mean air temperature. Simulations have been conducted to test these dimensions, with a focus on the flat plate as a controller. The impact of collector size on the mean air temperature is shown in Fig. 4, with example 8 showing a steady increase in temperature. Case 8, with dimensions of 1.8 m, 0.7 m, and 0.07 m, was selected for experimental and simulation investigations due to its cost-effectiveness. To improve heat transmission and increase surface area, a corrugated absorber plate is used instead of a flat plate in typical single-pass solar air heaters. The efficiency of solar air heaters can be significantly improved by modifying the heat absorber surface to increase airflow turbulence. One effective method is to install elements that disrupt airflow, such as small spheres, to enhance heat transfer and improve the friction coefficient [26].

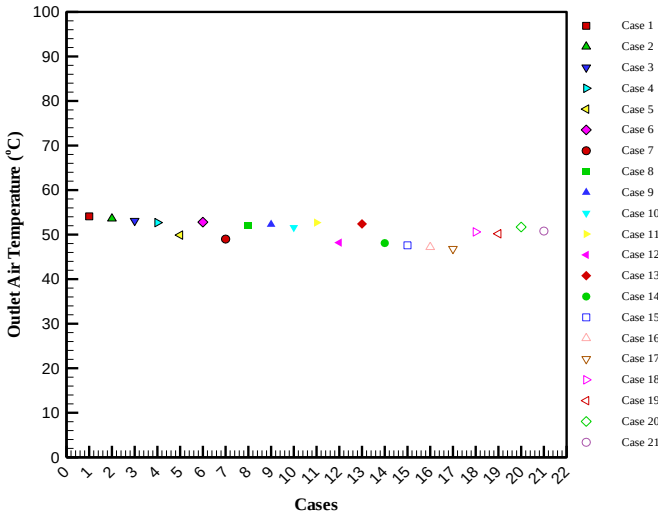

Figure 4. Plot of outlet air temperature vs SAH dimensions under 1000 W/m2 solar irradiation and 0.03 kg/s air mass flow rate

The performance of the SAH was evaluated for four distinct designs: flat plate, corrugated without storage, corrugated with PCM, and corrugated with Nano-PCM.

3.2 The thermal performance of the SAH flat panel was evaluated.

In this work, the thermal performance of a flat-plate solar air heater (SAH) with fixed dimensions (length = 1.8 m, width = 0.7 m, depth = 0.07 m) was evaluated using only air as the working fluid. The temperature differences between the air inlet and outlet were measured and plotted against the air mass flow rate. Fig. 5 shows the relationship between the temperature differences and different air mass flow rates (0.03–0.06 kg/s) when the collector was exposed to a constant solar irradiance of 1000 W/m². As the air mass flow rate increases, the air temperature difference decreases from 26.9 °C at 0.03 kg/s to 14 °C at 0.06 kg/s. The collector's thermal performance is quantified by the thermal efficiency, which accounts for the system's useful heat gain. Numerical analyses of the collector indicate that the thermal efficiency increases with increasing air mass flow rate, as shown in Fig. 6. Based on these results, the thermal efficiency of the collector at different air mass flow rates is summarized in Table 3.

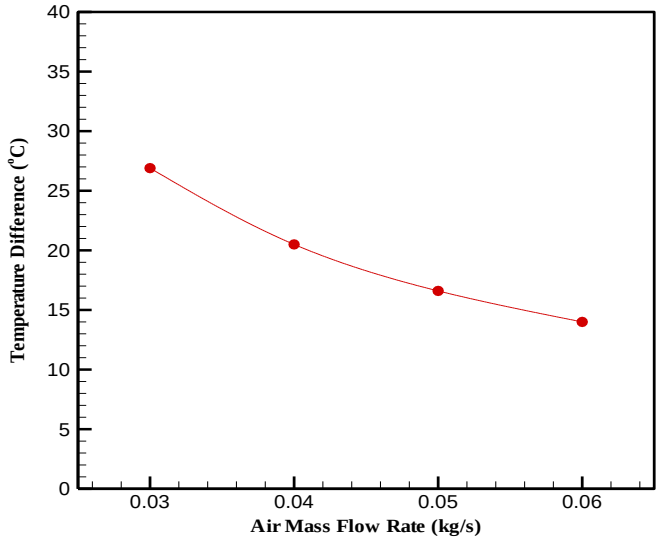

Figure 5. The change in air temperature difference with varying air mass flow rates over a flat solar array (SAH) of dimensions (L = 1.8 m, W = 0.7 m, Hch = 0.07 m) when exposed to a solar radiation of 1000 W/m².

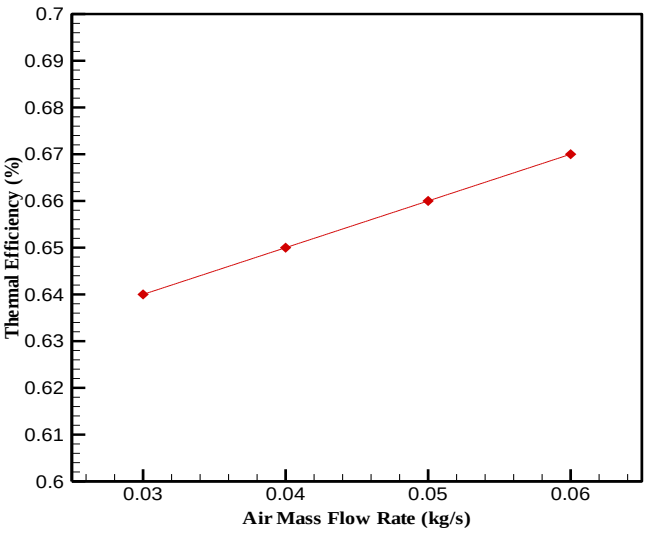

Figure 6. The efficiency of thermal management about varying air mass flow rates in a flat plate solar air heater operating at 1000 W/m2 of solar radiation with dimensions L = 1.8 m, W = 0.7 m, and Hch = 0.07 m.

Table 3. Situations were simulated to determine the optimal air-flow channel size for the collector.

Case	Dimensions of Collector L (m)	W (m)	H_{ch} (m)
1	1.9	0.8	0.08
2	1.9	0.8	0.07
3	1.9	0.8	0.06
4	1.9	0.7	0.08
5	1.9	0.6	0.08
6	1.9	0.7	0.07
7	1.9	0.6	0.06
8	1.8	0.7	0.07
9	1.8	0.7	0.08
10	1.8	0.7	0.06
11	1.8	0.8	0.07
12	1.8	0.6	0.07
13	1.8	0.8	0.08
14	1.8	0.6	0.06
15	1.7	0.6	0.08
16	1.7	0.6	0.07
17	1.7	0.6	0.06
18	1.7	0.8	0.06
19	1.7	0.7	0.06
20	1.7	0.8	0.08
21	1.7	0.7	0.07

In Fig. 4, we also observe the performance of the solar air heater (SAH) with dimensions of length, width, and height (1.8 meters, 0.7 meters, and 0.07 meters, respectively), at air flow rates ranging from (0.03 - 0.06 kg/s) under a solar irradiance of 1000 W/m².

Analysis of the simulation results shows that the air mass flow rate affects the transport fluid temperature and the temperature distribution within the airflow channel. Computational fluid dynamics (CFD) modeling was used for a flat-panel solar array (SAH) with dimensions of (L = 1.8 m, W = 0.7 m, and H_{ch} = 0.07 m), achieving a convergence criterion with a residual value of 10^{-4} after 90 iterations. Fig. 7 and 8 show the temperature distribution along the airflow channel of the flat-panel solar array. The CFD simulation results indicate that air temperature gradually increases along the channel, depending on the amount of heat transferred from the absorber plate to the air, as shown in Fig. 6.

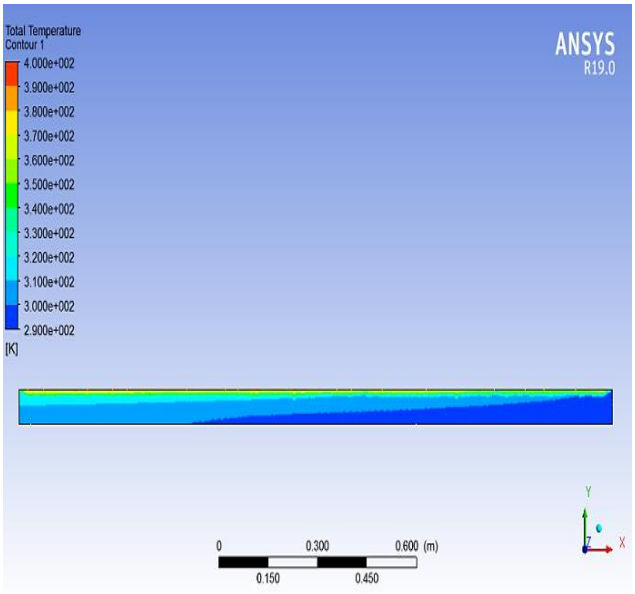

Figure 7. Side view of temperature distribution in a flat plate solar air heater (SAH) with dimensions: length 1.8 m, width 0.7 m, and duct height 0.07 m.

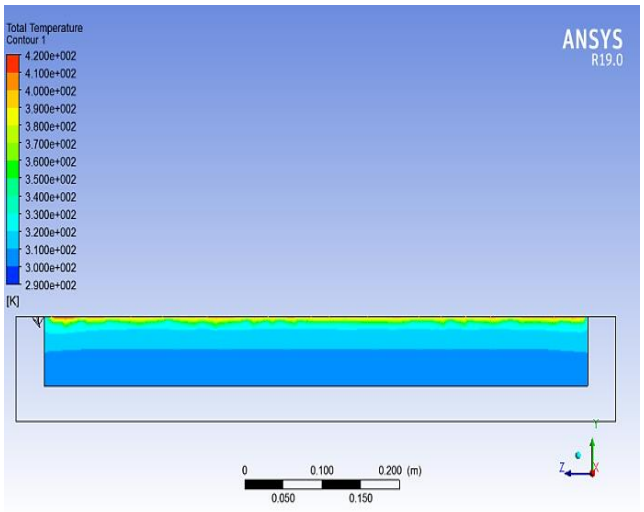

Figure 8. The distribution of air temperature at the outlet of a flat-plate solar collector array, which has dimensions of 1.8 meters in length, 0.7 meters in width, and a channel height of 0.07 meters.

Fig. 9 illustrates the variation in the air temperature difference at different mass flow rates (0.03–0.06 kg/s) for a corrugated solar air collector without a storage unit (SAH) with dimensions of 1.8 m length, 0.7 m width, and 0.07 m channel height, under a solar irradiance of 1000 W/m². The figure shows that as the air mass flow rate increases, the temperature difference decreases. This is because increasing the air flow through the collector distributes the same thermal energy over a larger mass of air, thereby reducing the temperature rise. For example, at an air mass flow rate of 0.03 kg/s, the temperature difference is 62.0 °C, while it decreases to 33.1 °C at 0.06 kg/s.

The thermal efficiency of the corrugated collector without a storage unit, with similar dimensions and under the same solar irradiance, was evaluated at air mass flow rates between 0.03 and 0.06 kg/s, and the numerical results, expressed in W/m², are shown in Fig. 10

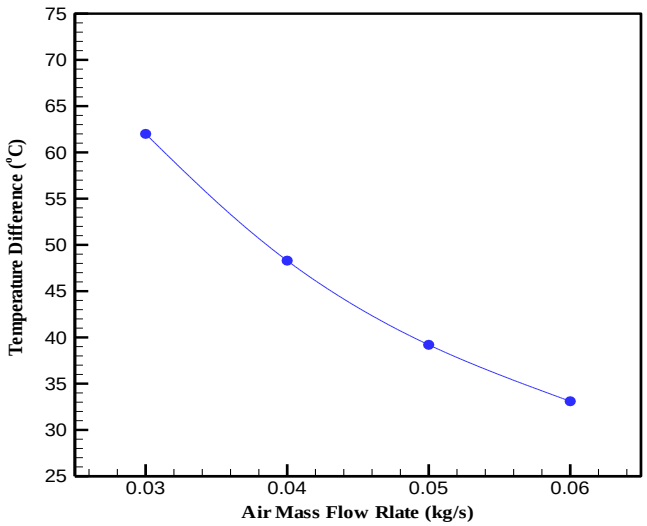

Figure 9. The difference in air temperature at different mass flow rates for a corrugated solar air heater (SAH) without a storage unit, with dimensions L = 1.8 meters, W = 0.7 meters, and channel height Hch = 0.07 meters, under a solar irradiance of 1000 W/m².

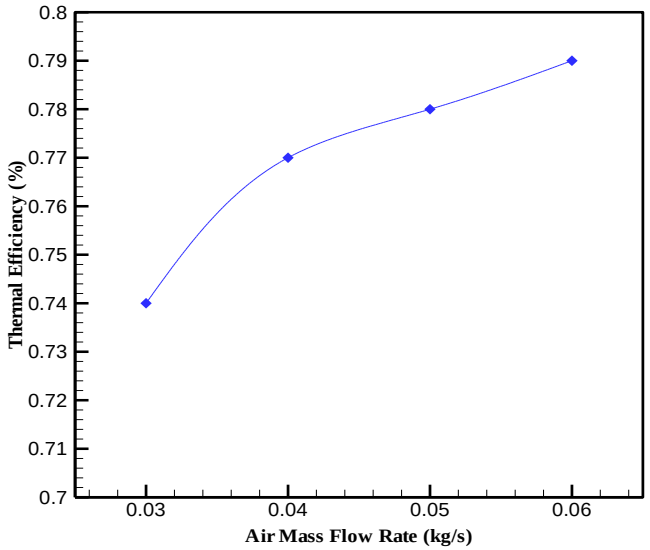

Figure 10. The study demonstrates the relationship between thermal efficiency and air mass flow rate for a non-storage corrugated solar panel (SAH) with dimensions (L = 1.8 m, W = 0.7 m, Hch = 0.07 m) when exposed to a solar radiation of 1000 W/m².

Convergence criteria for the corrugated air-discharge iteration pattern were determined using a storage-free CFD simulation with 150 iterations and a residual target of 10^{-4}, for dimensions L = 1.8 m, W = 0.7 m, and Hch = 0.07 m. Fig. 11 and 12 show the temperature distribution along the ventilation duct in a storage-free corrugated air discharge system with the exact

dimensions. It is evident that temperature affects the absorber plate; therefore, increased conductive heat transfer to the absorber plate raises the temperature of the outflow air.

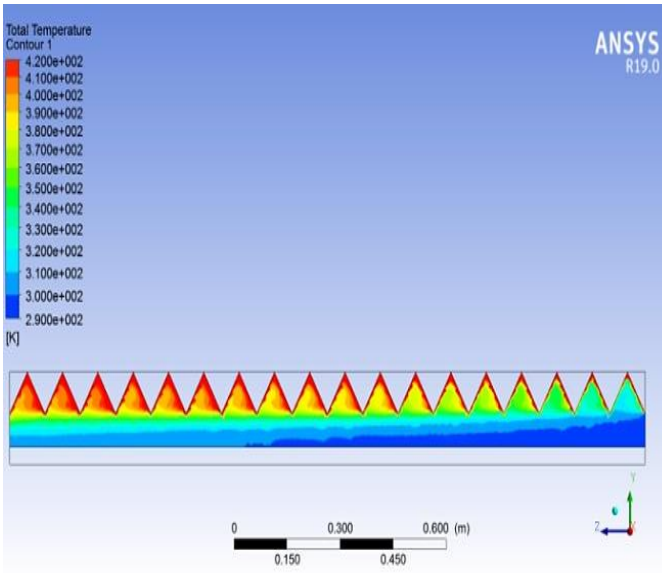

Figure 11. The dimensions of the side image depict the temperature distribution of unstored corrugated SAH: L = 1.8 m, W = 0.7 m, Hch = 0.07 m.

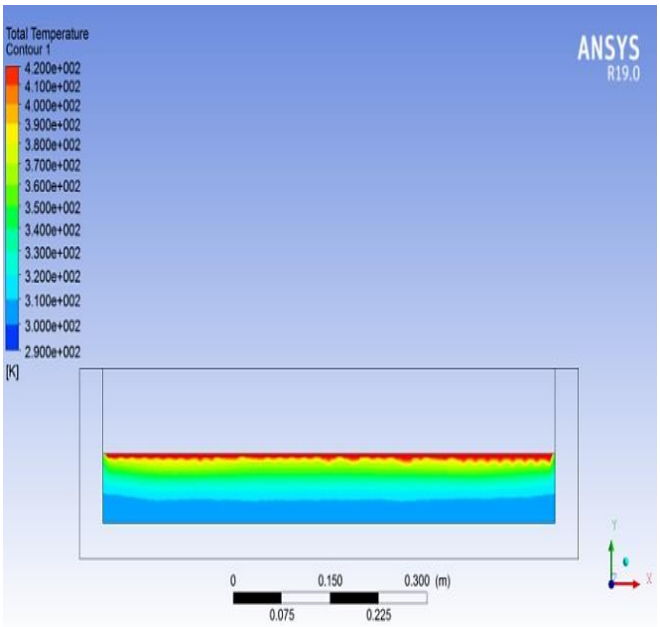

Figure 12. The temperature distribution for the following dimensions: L = 1.8 m, W = 0.7 m, Hch = 0.07 m.

When a corrugated solar panel equipped with phase change materials (SAH with PCM) is exposed to a solar radiation of 1000 W/m² and has dimensions (length = 1.8 m, width = 0.7 m, and duct height = 0.07 m), Fig. 13 shows the relationship between the air temperature difference and different air mass flow rates (0.03–0.06 kg/s). The graph shows a decrease in the air temperature difference with increasing air mass flow rate, from 44.0°C to 23.5°C as the flow rate increases from 0.03 kg/s to 0.06 kg/s under the same irradiance.

The numerical results for the thermal efficiency in Fig. 14 also show the effect of different air mass flow rates on the thermal performance of a corrugated roof (SAH with PCM). The results demonstrate that as the air mass flow rate increases, the thermal efficiency rises significantly, indicating improved heat transfer from the panel to the air.

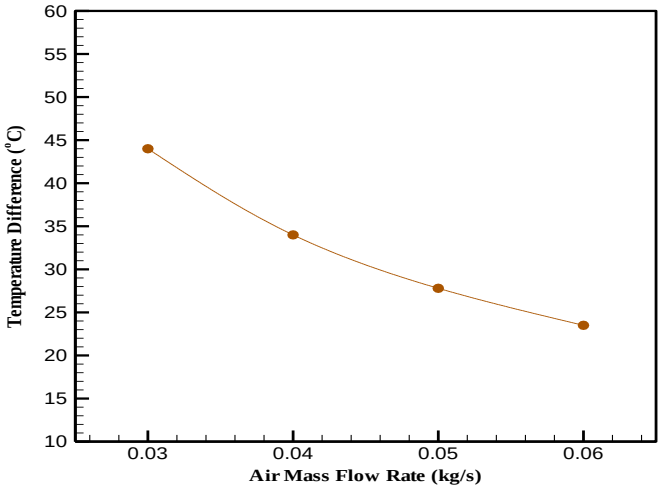

Figure 13. The dimensions of a corrugated solar panel with phase change material (SAH with PCM) are shown as follows: length = 1.8 m, width = 0.7 m, and duct height = 0.07 m, operating under a solar irradiance of 1000 W/m². The figure also shows the relationship between air temperature difference and various air mass flow rates.

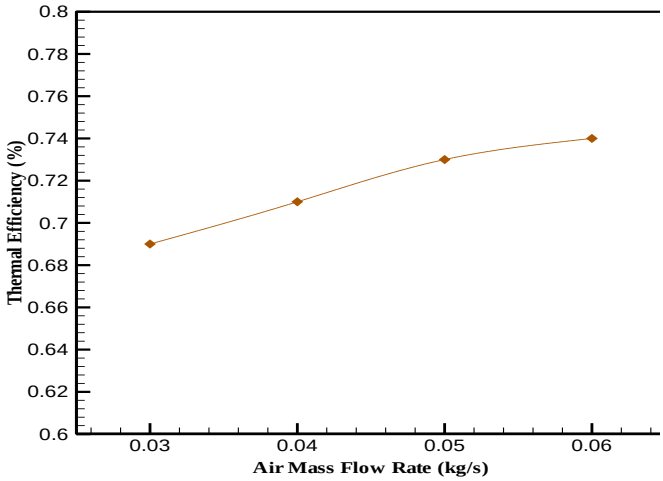

Figure 14. Corrugated solar panels with phase change material (SAH with PCM) with dimensions (L = 1.8 m, W = 0.7 m, Hch = 0.07 m) and under a solar irradiance of 1000 W/m² show the temperature variation as a function of different air mass flow rates.

The convergence criterion of the solutions for the simulation model was determined using computational fluid dynamics (CFD) for a corrugated solar panel with phase change material (SAH with PCM) at 180 iterations and a residual target of 10^{-4}, for dimensions L = 1.8 m, W = 0.7 m, and Hch = 0.07 m. Fig.

15 and 16 show the temperature distribution along the airflow channel in this system with the exact dimensions.

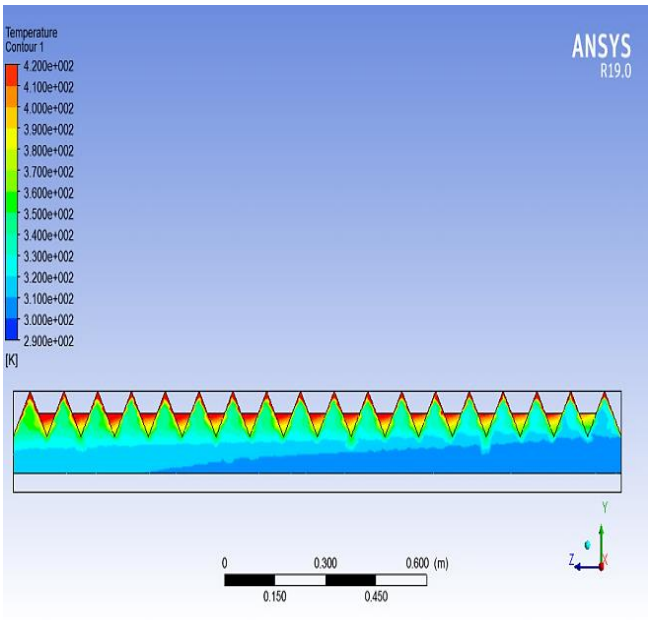

Figure 15. The temperature distribution of the corrugated SAH with PCM is depicted in this side view. The dimensions of the SAH are as follows: L = 1.8 m, W = 0.7 m, Hch = 0.07 m.

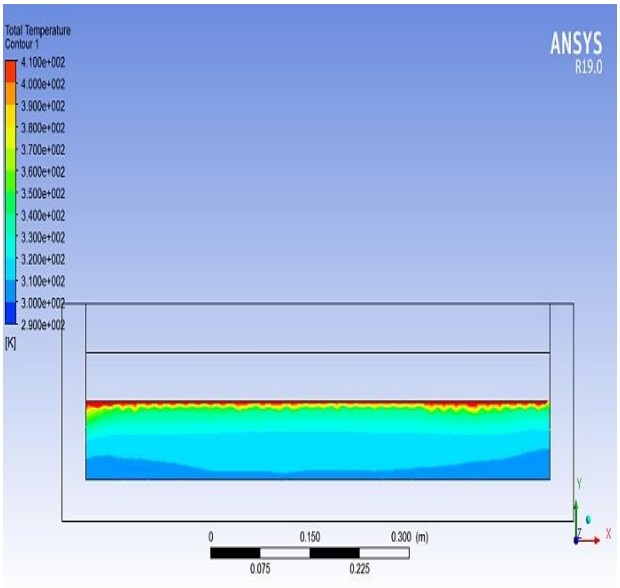

Figure 16. The air section exiting a corrugated solar panel with phase change material (SAH with PCM) shows the temperature distribution for dimensions: L = 1.8 m, W = 0.7 m, and Hch = 0.07 m.

Fig. 17 shows the relationship between the air temperature difference and different air mass flow rates (0.03–0.06 kg/s) for a corrugated solar roof with nano-PCM dimensions (length = 1.8 m, width = 0.7 m, and duct height = 0.07 m) under a solar radiation of 1000 W/m². The figure shows that increasing the air mass flow rate reduces the temperature difference, which decreased from 46.4°C to 25.0°C as the flow rate increased from 0.03 kg/s to 0.06 kg/s under a solar radiation of 600 W/m².

Fig. 18 also shows the numerical results for the thermal efficiency at different air mass flow rates, with a solar irradiance of 1000 W/m², for a corrugated SAH panel with Nano-PCM (L = 1.8 m, W = 0.7 m, Hch = 0.07 m). The results show that increasing the air mass flow rate significantly improves the thermal efficiency, as shown in Fig. 18.

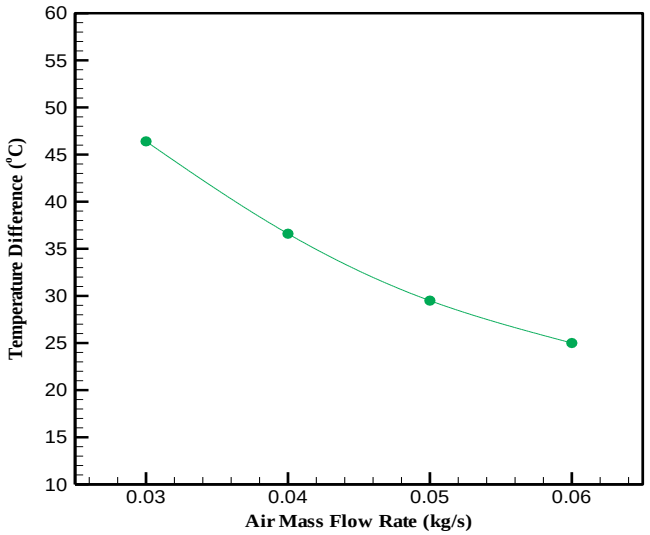

Figure 17. This side view shows the temperature distribution of a corrugated solar panel with phase change material (SAH with PCM) with dimensions (L = 1.8 m, W = 0.7 m, Hch = 0.07 m).

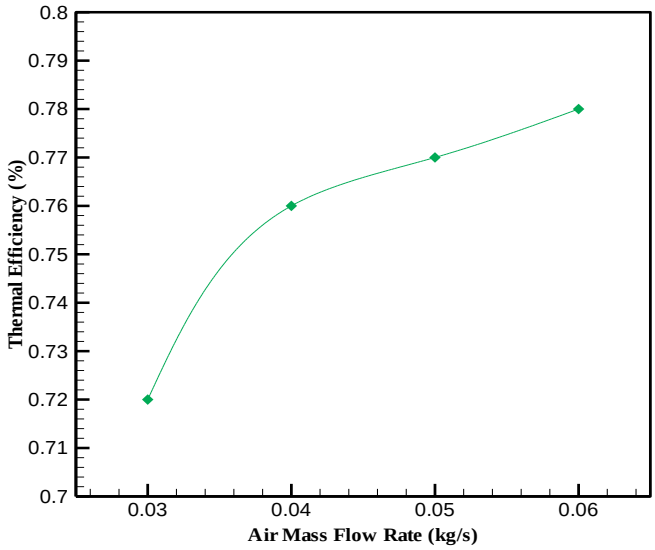

Figure 18. The figure shows the temperature distribution in the air exiting a corrugated solar panel with phase change material (SAH with PCM) for dimensions: L = 1.8 m, W = 0.7 m, and Hch = 0.07 m.

The convergence criterion was achieved with a residual of 10^{-4} after 190 iterations in the computational fluid dynamics (CFD) simulation of a corrugated solar panel with a nano-PCM, with dimensions (L = 1.8 m, W = 0.7 m, Hch = 0.07 m). Fig. 19 and

20 show the temperature distribution in a corrugated panel with nano-PCM, with the exact dimensions.

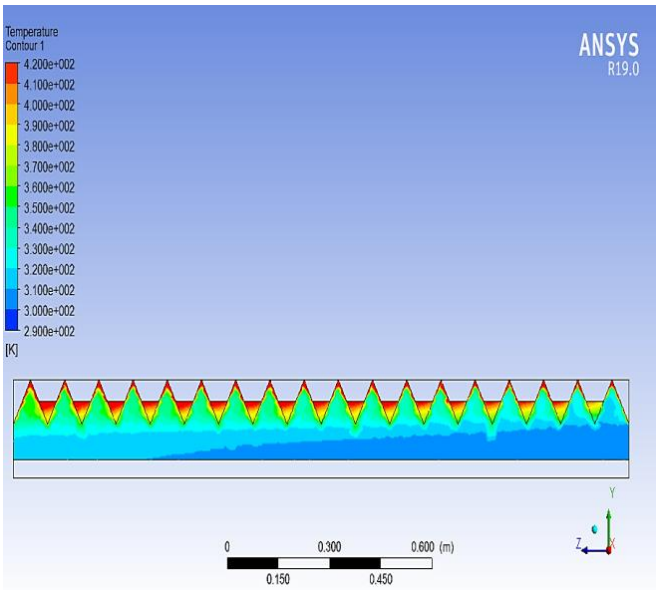

Figure 19. The figure shows the temperature distribution on the side of a corrugated solar panel equipped with Nano-PCM (SAH) with dimensions (L = 1.8 m, W = 0.7 m, Hch = 0.07 m).

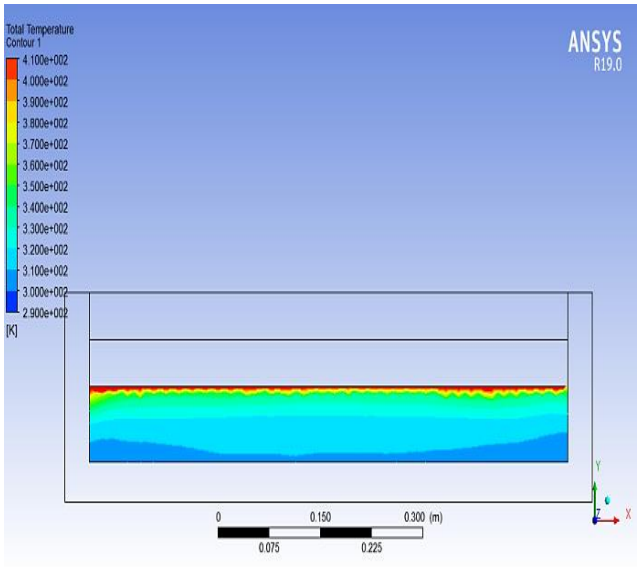

Figure 20. The figure shows the temperature distribution in the air exiting a corrugated solar panel equipped with Nano-PCM (SAH) with dimensions (L = 1.8 m, W = 0.7 m, Hch = 0.07 m).

Results from numerical analyses across all scenarios indicate that increasing the air mass flow rate improves thermal efficiency. By contrast, the output air temperature decreases. This could be because a lower heat-transfer coefficient results from a decrease in plate temperature as the air mass flow rate increases.

4 Conclusions

The numerical results indicate that the design configuration is the primary determinant of the optimal collector dimensions. Here are the elements that shaped the design: the collector dimensions, which play an essential role in achieving high efficiency. The collector dimensions have been selected to achieve optimal performance while accounting for cost. The collector dimensions (L = 1.8 m, W = 0.7 m, Hch = 0.07 m) were adopted as the best design for the solar air-cooled collector (SAH).

Nanoparticles: - nanoparticles enhance the performance of SAH compared to the pure paraffin wax. It was demonstrated that the SAH with Nano-PCM exhibited the highest heat-transfer coefficient. This is followed by presentations of the corrugated solar panel with phase change material (SAH with PCM) and the solar panel without storage (SAH without storage). Al_2O_3 nanoparticles with paraffin wax increased the average air temperature difference and thermal efficiency. This phenomenon can be attributed to the higher thermo-physical properties of Al2O3-paraffin wax relative to those of pure paraffin wax.

Acknowledgment.

Thanks to Al-Furat Al-Awsat Technical University - Technical Institute/Najaf for providing the scientific laboratories and expertise to complete the work requirements.

Nomenclature

The symbol	Symbols name
$\dot{m}$	Air mass flow rate (kg/s)
ρ	Density (kg/m^3)
H_{ch}	Depth of airflow channel (m)
μ	Dynamic viscosity (kg/m s)
μ_t	Eddy viscosity (kg/m s)
u_i'	Fluctuation velocity components (m/s)
in	Inlet temperature (°C)
L	Length of the collector (m)
Γ	Molecular thermal diffusivity (m^2/s)
u	Mean velocity (m/s)
out	Outlet temperature (°C)
PCM	Phase change material
SAH	Solar air heater
T	Temperature (°C)
k	Thermal conductivity (W/m K)
η_{th}	Thermal efficiency (%)
C_μ	Turbulence model constant
ε	Turbulent dissipation rate (m^2/s^3)
Γ_t	Turbulent thermal diffusivity (m^2/s)
W	Width of the collector (m)

Conflict of interest

Ahmed Hammodi Abd, Hazim A. Al-Zurfi, and K. Sopian declare that they have no conflicts of interest.

Author Contribution Statement

Hammodi Abd and Hazim A. Al-Zurfi: Proposed the problem statement, verified the analytical methods, and investigated and supervised.

Layth Mustafa Salman and K. Sopian: Developed the theory and performed the computations.

References

[1] Z. N. Suzah, A. J. Hamad, and A. Hadi, "Performance Enhancement of Double-Pass Solar Air Heater Using Phase Change Materials and Air Flow Turbulators," *Journal of Engineering and Sustainable Development*, vol. 29, no. 5, pp. 598–607, Aug. 2025, doi: https://doi.org/10.31272/jeasd.2498

[2] S. A. Hussein and M. A. Nima, "Numerical and Experimental Investigation of Semicircular Solar Updraft Tower System Employing Porous Copper Metal Foam," *Journal of Engineering and Sustainable Development*, vol. 27, no. 5, pp. 596–614, Sep. 2023, doi: https://doi.org/10.31272/jeasd.27.5.4

[3] W. Lin, W. Gao, and T. Liu, "A Parametric Study on the Thermal Performance of cross-corrugated Solar Air Collectors," *Applied Thermal Engineering*, vol. 26, no. 10, pp. 1043–1053, Jul. 2006, doi: https://doi.org/10.1016/j.applthermaleng.2005.10.005

[4] A. A. El-Sebaii, S. Aboul-Enein, M. R. I. Ramadan, S. M. Shalaby, and B. M. Moharram, "Thermal Performance Investigation of Double Pass-Finned Plate Solar Air Heater," *Applied Energy*, vol. 88, no. 5, pp. 1727–1739, May 2011, doi: https://doi.org/10.1016/j.apenergy.2010.11.017

[5] M. A. Karim, E. Perez, and Z. M. Amin, "Mathematical Modelling of Counter Flow v-grove Solar Air Collector," *Renewable Energy*, vol. 67, pp. 192–201, Jul. 2014, doi: https://doi.org/10.1016/j.renene.2013.11.027

[6] A. Al-Damook and W. H. Khalil, "Experimental Evaluation of an Unglazed Solar Air Collector for Building Space Heating in Iraq," *Renewable Energy*, vol. 112, pp. 498–509, May 2017, doi: https://doi.org/10.1016/j.renene.2017.05.051

[7] A. M. Aboghrara, B. T. H. T. Baharudin, M. A. Alghoul, N. M. Adam, A. A. Hairuddin, and H. A. Hasan, "Performance Analysis of Solar Air Heater with Jet Impingement on Corrugated Absorber Plate," *Case Studies in Thermal Engineering*, vol. 10, pp. 111–120, Sep. 2017, doi: https://doi.org/10.1016/j.csite.2017.04.002

[8] H. Hassan and S. Abo-Elfadl, "Experimental Study on the Performance of Double Pass and Two Inlet Ports Solar Air Heater (SAH) at Different Configurations of the Absorber Plate," *Renewable Energy*, vol. 116, pp. 728–740, Sep. 2017, doi: https://doi.org/10.1016/j.renene.2017.09.047

[9] P. Charvat, M. Ostry, T. Mauder, and L. Klimes, "A Solar Air Collector with Integrated Latent Heat Thermal Storage," *EPJ Web of Conferences*, vol. 25, p. 01028, 2012, doi: https://doi.org/10.1051/epjconf/20122501028

[10] C. Zauner, F. Hengstberger, B. Mörzinger, R. Hofmann, and H. Walter, "Experimental Characterization and Simulation of a Hybrid sensible-latent Heat Storage," *Applied Energy*, vol. 189, pp. 506–519, Mar. 2017, doi: https://doi.org/10.1016/j.apenergy.2016.12.079

[11] B. S. Albusoda, "Engineering Assessments of Liquefaction Potential Baghdad Soil Under Dynamic Loading", *Journal of Engineering and Sustainable Development*, vol. 20, no. 1, pp. 59–76, Jan. 2016, Accessed: Oct. 03, 2025. Available: https://jeasd.uomustansiriyah.edu.iq/index.php/jeasd/article/view/631

[12] S. Vijayan, T. V. Arjunan, and A. Kumar, "Mathematical Modeling and Performance Analysis of Thin Layer Drying of Bitter Gourd in Sensible Storage Based Indirect Solar Dryer," *Innovative Food Science & Emerging Technologies*, vol. 36, pp. 59–67, Aug. 2016, doi: https://doi.org/10.1016/j.ifset.2016.05.014

[13] H. M. Ali, Radhi Abdullah Lawag, M. Indra, and Islam, "RT 42 and RT 50 Phase Change materials-based Heat Sinks for Thermal Management of Electronics," *Journal of Thermal Analysis and Calorimetry*, vol. 150, no. 5, pp. 3463–3473, Feb. 2025, doi: https://doi.org/10.1007/s10973-024-13708-1

[14] D. V. N. Lakshmi, A. Layek, and P. M. Kumar, "Performance Analysis of Trapezoidal Corrugated Solar Air Heater with Sensible Heat Storage Material," *Energy Procedia*, vol. 109, pp. 463–470, Mar. 2017, doi: https://doi.org/10.1016/j.egypro.2017.03.069

[15] G. Alva, Y. Lin, and G. Fang, "An Overview of Thermal Energy Storage Systems," *Energy*, vol. 144, pp. 341–378, Feb. 2018, doi: https://doi.org/10.1016/j.energy.2017.12.037

[16] R. Tchinda, "A Review of the Mathematical Models for Predicting Solar Air Heaters Systems," *Renewable and Sustainable Energy Reviews*, vol. 13, no. 8, pp. 1734–1759, Oct. 2009, doi: https://doi.org/10.1016/j.rser.2009.01.008

[17] A. Mahmud, K. Sopian, M. A. Alghoul, Mat Sohif, and A. M. Graisa, "Using a Paraffin Wax-Aluminum Compound as a Thermal Storage Material in a Solar Air Heater," *Journal of Engineering and Applied Sciences*, vol. 4, no. 10, pp. 74–77, Dec. 2009, Accessed: Jul. 21, 2025. [Online]. Available: https://pure.kfupm.edu.sa/en/publications/using-a-paraffin-wax-aluminum-compound-as-a-thermal-storage-mater

[18] M. M. Alkilani, K. Sopian, and S. Mat, "Fabrication and Experimental Investigation of PCM Capsules Integrated in Solar Air Heater," *American Journal of Environmental Sciences*, vol. 7, no. 6, pp. 542–546, Oct. 2011, doi: https://doi.org/10.3844/ajessp.2011.542.546.

[19] N. S. Dhaidan, J. M. Khodadadi, T. A. Al-Hattab, and S. M. Al-Mashat, "Experimental and Numerical Investigation of Melting of NePCM inside an Annular Container under a Constant Heat Flux Including the Effect of Eccentricity," *International Journal of Heat and Mass Transfer*, vol. 67, pp. 455–468, Dec. 2013, doi: https://doi.org/10.1016/j.ijheatmasstransfer.2013.08.002

[20] B. J. Nabhan, "Using Nanoparticles for Enhance Thermal Conductivity of Latent Heat Thermal Energy Storage," *Journal of Engineering*, vol. 21, no. 6, pp. 37–51, Jun. 2015, doi: https://doi.org/10.31026/j.eng.2015.06.03

[21] B. Salman and H. Obaid, "Enhanced Performance of Flat Plate Solar Collector with Twisted Tape Double Cutting Rectangle Shape," *Journal of Engineering and Sustainable Development*, vol. 29, no. 1, pp. 68–78, Jan. 2025, doi: https://doi.org/10.31272/jeasd.3128

[22] A. Aljumaili, Y. Alaiwi, and Z. Al-Khafaji, "Investigating back surface cooling system using phase change materials and heatsink on photovoltaic performance," *Journal of Engineering and Sustainable Development*, vol. 28, no. 3, pp. 294–315, May 2024, doi: 10.31272/jeasd. 28.3.1.

[23] W. Su, J. Darkwa, and G. Kokogiannakis, "Development of Microencapsulated Phase Change Material for Solar Thermal Energy Storage," *Applied Thermal Engineering*, vol. 112, pp. 1205–1212, Feb. 2017, doi: https://doi.org/10.1016/j.applthermaleng.2016.11.009

[24] S. Eiamsa-ard and P. Promvonge, "Numerical Study on Heat Transfer of Turbulent Channel Flow over Periodic Grooves," *International Communications in Heat and Mass Transfer*, vol. 35, no. 7, pp. 844–852, Aug. 2008, doi: https://doi.org/10.1016/j.icheatmasstransfer.2008.03.008

[25] T. M. Soe and S. Y. Khaing, "Comparison of Turbulence Models for Computational Fluid Dynamics Simulation of Wind Flow on a Cluster of Buildings in Mandalay," *International Journal of Scientific and Research Publications*, vol. 7, no. 8, pp. 337–350, 2017, Available: https://www.ijsrp.org/research-paper-0817.php?rp=P686711

[26] A. M. Abdulmalik, B. Freegah, B. S. Khalaf, and M. H. Alhamdo, "Heat Transfer Inside Building- Cladding Solar Collector," *Journal of Engineering and Sustainable Development*, vol. 24, no. 4, pp. 26–34, Jul. 2020, doi: https://doi.org/10.31272/jeasd.24.4.4